

Photoacoustic and optical absorption spectroscopy studies of luminescent Cr^{3+} and Cr^{4+} centers in yttrium aluminum garnet

M. Grinberg, A. Sikorska, A. Śliwiński, and J. Barzowska
Institute of Experimental Physics, University of Gdansk, Wita Stwosza 57, Gdansk, Poland

Y. R. Shen
Department of Chemistry, Washington State University, Pullman, Washington 99164

S. B. Ubizskii
Institute for Telecommunication, Radioelectronics and Electronic Engineering, Lviv Polytechnic National University, 12, Bandera St., Lviv, 79013, Ukraine

S. S. Melnyk
R&D Institute for Materials, Scientific Research Company "Carat," 202, Stryjska St., Lviv, 79031, Ukraine

(Received 23 May 2002; published 31 January 2003)

We present the experimental results for photoacoustic and optical absorption spectra of as-grown, air-annealed, and hydrogen-annealed yttrium aluminum garnet (YAG):Cr,Mg crystals. The experimental results were analyzed and discussed for both Cr^{3+} and Cr^{4+} centers in the host lattice within the framework of the Rosenzweig-Gersho (RG) theory that was extended by considering the existence of radiative processes in the emitting centers. The extended RG theory reasonably predicted a low and excitation-energy-independent quantum efficiency for Cr^{4+} centers in YAG but failed in the case of high-field Cr^{3+} centers in YAG that contain a long-lived emitting state (2E) unless the quantum efficiency of Cr^{3+} is assumed to increase with increasing excitation energy.

DOI: 10.1103/PhysRevB.67.045113

PACS number(s): 78.55.Hx, 71.70.Ch, 62.50.+p

I. INTRODUCTION

Yttrium aluminum garnet [$\text{Y}_3\text{Al}_5\text{O}_{12}$ (YAG)] single crystals are widely used as a solid state laser host medium. In YAG crystals, chromium ion such as Cr^{3+} can occupy octahedrally coordinated Al^{3+} sites or Cr^{4+} tetrahedrally coordinated Al^{3+} sites. Cr^{4+} in YAG exhibits a near-infrared (NIR) luminescence broadband safe for the eye and potentially applicable in medicine.¹⁻³ The Cr^{4+} NIR luminescence process in YAG is accompanied by a strong nonradiative relaxation. Since Cr^{3+} ions always coexist in Cr^{4+} systems, the investigations of YAG material systems containing only Cr^{3+} and a Cr^{3+} and Cr^{4+} mixture in different ratios are crucial to improving the Cr^{4+} lasing efficiency because competitive processes and mutual interactions between Cr^{4+} and Cr^{3+} ions occur.

Photoacoustic spectroscopy, one of the photothermal techniques, provides an efficient tool for one to directly investigate nonradiative processes of optical materials. A basic assumption used for the interpretation of the photoacoustic signal (PAS) is that the heat is generated at the place where the light is absorbed. For point centers, this assumption allows one to directly relate the PAS spectra to the characteristic absorption spectra of the centers. Some recent papers⁴⁻⁹ have reported PAS results for comparison with optical absorption results in garnet crystals doped with cerium ions⁴ and chromium ions,⁵⁻⁹ and discussed the relative quantum efficiency of the systems as a function of excitation energy.

A localized system after highly excited nonradiatively relaxes to its first excited state and behaves more or less meta-

stable. After reaching a thermal equilibrium in the metastable excited state, the system can further relax to its ground state in radiative and/or nonradiative ways. In the strong electron-lattice coupling case, internal conversion processes can non-radiatively convert the energy from the excited vibronic states of the excited electronic manifold to the ground electronic manifold before the excited system reaches thermal equilibrium. A theoretical model that describes the kinetics of nonradiative processes and is used to determine the quantum efficiency of excited systems has been proposed by Grinberg and Mandelis¹⁰⁻¹² for analysis of photopyroelectric data. This model was later extended for analysis of photoacoustic spectroscopy⁴ and also successfully applied for analysis of the relation between photoacoustic and absorption spectra of chromium doped $\text{Y}_3\text{Ga}_5\text{O}_{12}$ (YGG) and YAG crystals.^{6,7}

In this paper, we present and discuss experimental results for photoacoustic and optical absorption spectroscopy in YAG crystals doped with chromium and magnesium. We modify relative concentrations of trivalent and tetravalent chromium ions (Cr^{3+} and Cr^{4+}) by the use of heat annealing treatments in air and hydrogen atmosphere. Next we establish a quantitative relation between the optical absorption and photoacoustic spectra in the context of the abovementioned model for the kinetics of nonradiative relaxation processes¹² and a standard Rosenzweig-Gersho theory for photoacoustic processes.¹³

II. TRIVALENT AND TETRAVALENT CHROMIUM ELECTRONIC STRUCTURES

Cr^{4+} and Cr^{3+} ions are occupied by two and three d electrons, respectively. In standard crystal field theory, elec-

tronic structures and optical properties of Cr^{4+} and Cr^{3+} ions are essentially governed by crystal fields and spin-orbit interactions. In both the Cr^{3+} and Cr^{4+} cases, their electronic structures are graphically given by Tanabe-Sugano diagrams of d^2 and d^3 ions in a cubic approximation¹⁴ and described by two Racach parameters (B and C) and one crystal field strength ($10Dq$). In the ground state, both systems are characterized by a high spin state ($S=1$ for d^2 systems and $S=3/2$ for d^3 systems). The octahedrally coordinated Cr^{3+} ion has the t_2^3 ground electronic configuration whereas the tetrahedrally coordinated Cr^{4+} ion has the e^2 ground electronic configuration. Both ions can be excited in two ways: either by reversing the spin of one electron or exciting one electron to excited electronic configurations without changing the spin. Cr^{3+} ion has the 4A_2 ground state and its first excited state depending on the crystal field strength is either 4T_2 ($Dq/B < 2.4$, low field) or 2E ($Dq/B > 2.4$, high field). The 2E excited state and the 4A_2 ground state of Cr^{3+} belong to the t_2^3 ground electronic configuration whereas the 4T_2 excited state belongs to the t_2^2e excited electronic configuration. The higher excited states are two 2T_1 and 2T_2 doublets belonging to the t_2^3 ground electronic configuration and two $^4T_{1a}$ and $^4T_{1b}$ quartets belonging to the t_2^2e and t_2e^2 excited electronic configurations, respectively. The Cr^{4+} ion has the 3A_2 ground state and its first excited state depending on the crystal field strength is either 3T_2 ($Dq/B < 2.7$, low field) or 1E ($Dq/B > 2.7$, high field). The 1E excited state and the 3A_2 ground state of Cr^{4+} belong to the e^2 ground electronic configuration whereas the 3T_2 excited state belongs to the et_2 first excited electronic configuration. The 1E and 1A_1 excited states also belong to the e^2 ground electronic configuration. The $^3T_{1a}$ and $^3T_{1b}$ excited states are originated from the et_2 first and t_2^2 second excited electronic configuration, respectively. In YAG, Cr^{3+} ion is in strong field and Cr^{4+} ion in weak field.^{3,15,16}

When a system is excited from its ground electronic configuration to one of its excited electronic configurations, a change in the electron distribution leads to the rearrangement of ligand ions. This is due to the fact that negative ligands have to shift in response to the change in the d -electron charge density. As a result, the energy of the system after excitation is lost with the quantity of $S\hbar\omega$, where S is the Huang and Rhys factor and $\hbar\omega$ is the energy of the local phonon mode. This effect can be intuitively represented by a configurational coordinate diagram. Figures 1(a) and 1(b) show the diagrams for Cr^{4+} and Cr^{3+} ions, respectively. According to the spin selection rule, transitions occur preferentially between the same spin states. This is a reason why Cr^{3+} ion exhibits dominant absorption transitions between the ground state (4A_2) and the excited quartet states (4T_2 , $^4T_{1a}$, and $^4T_{1b}$) and Cr^{4+} ion exhibits dominant absorption transitions between the ground state (3A_2) and the excited triplet states (3T_2 , $^3T_{1a}$, and $^3T_{1b}$).

Cr^{3+} and Cr^{4+} ions in YAG after excitation relax nonradiatively to the first 2E excited state and the first 3T_2 excited state, respectively. The Cr^{3+} system shows long-lived R line luminescence that originates from a spin forbidden $^2E \rightarrow ^4A_2$ transition and can be observed at all temperatures.¹⁷

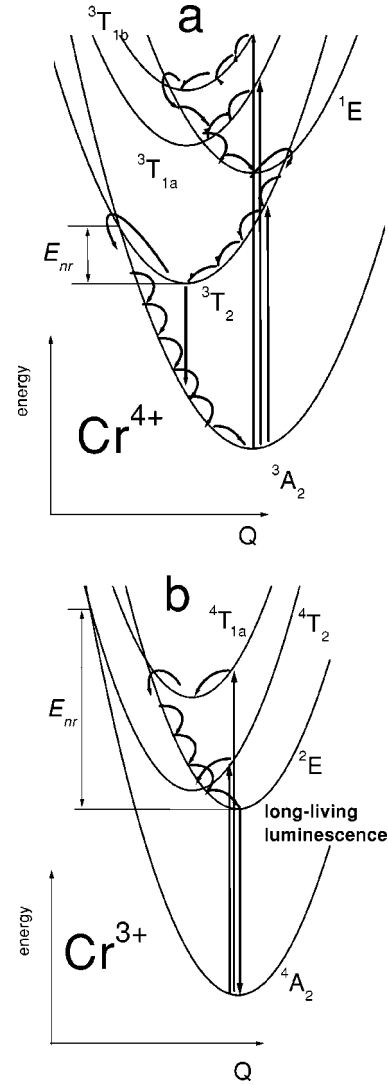


FIG. 1. Configurational coordinate diagrams for (a) Cr^{4+} and (b) Cr^{3+} .

The R line luminescence of Cr^{3+} in YAG has a temperature-dependent lifetime (from ~ 3 ms at room temperature to ~ 9 ms at 20 K).¹⁷ The temperature-dependent R line luminescence lifetime is mainly due to the variation of population with temperature in the higher excited vibronic states of the 2E state and the 4T_2 excited state that have a larger radiative transition rate. The higher vibronic states of the 2E electronic manifold are mixed with the 4T_2 state through the spin-orbit coupling.¹⁸ The Cr^{4+} system shows a weak $^3T_2 \rightarrow ^3A_2$ emission whose lifetime is temperature dependent (from $\sim 2 \mu\text{s}$ at room temperature to $\sim 30 \mu\text{s}$ at 20 K in YAG: Cr^{4+}).¹⁹ The strong decrease in the Cr^{4+} lifetime with increasing temperature is mainly due to nonradiative internal conversion processes.

III. PHOTOACOUSTIC SIGNAL AND EFFICIENCY OF NONRADIATIVE TRANSITIONS

PAS signals originate from the generation of heat flux in system excited by a modulated light beam of an excitation

wavelength of λ (the excitation energy of $\hbar\Omega$) and a modulation frequency of f . The periodical heat flux causes periodical variations of the sample surface temperature and consequently generates the overpressure (registered with a microphone) in a gas-filled photoacoustic cell (PAC). When $l_s \gg \mu_s$, where l_s and μ_s are the sample thickness and the thermal diffusion length, respectively, the Rosencwaig-Gersho theory,¹³ refined later by McDonald and Wetsel,²⁰ yields the following expression for complex PAS signal amplitudes:

$$P = -\frac{iI_0 p_0}{4\pi f l_g \rho c_v} \left\{ \frac{\beta}{\sigma_s T_0 (g+1)(r+1)} + \xi [1 - \exp(-\beta l_s)] \right\}, \quad (1)$$

where I_0 is the incident light intensity, p_0 and T_0 are ambient pressure and room temperature, respectively, c_v is the heat capacity of the sample, l_g and l_s are the thickness of the gas layer and the sample in the PAC, respectively, and β , ρ , and ξ are the absorption coefficient, the density, and the thermal expansion coefficient of the sample, respectively. g , r and σ_s are complex quantities given by

$$g = \frac{k_g a_g}{k_s a_s}, \quad r = (1-i) \frac{\beta}{2a_s}, \quad \sigma_s = (1+i)a_s, \quad (2)$$

where k_g and a_g are the thermal conductivity and the thermal diffusion coefficient of the gas in the PAC, respectively. k_s and a_s are the thermal conductivity and thermal diffusion coefficient of the sample, respectively. Thermal diffusion coefficients are a functions of the modulation frequency (f):

$$a_i = \mu_i^{-1} = \sqrt{\frac{2\pi f}{2\alpha_i}}, \quad (3)$$

where α_i ($i=s, g$) is the thermal diffusivity and μ_i is thermal diffusion length.

In the original Rosencwaig-Gersho model for solids,¹³ it has been assumed that the relaxation process in the sample is purely nonradiative and instantaneous within the period of the light modulation. When a system simultaneously includes nonradiative and radiative processes, the excitation or absorbed energy ($E_{\text{ex}} = \hbar\Omega$) is not fully converted to heat and photoemissive effects are therefore taken into account in analysis of the PAS signals. The optical to thermal energy conversion efficiency [$\eta_{\text{NR}}^{(e)}(\hbar\Omega, T)$] is given by

$$\eta_{\text{NR}}^{(e)}(\hbar\Omega, T) = \frac{Q}{\hbar\Omega} \quad (4)$$

where Q is the heat energy converted from the absorbed energy and T is the absolute temperature.

When we deal with fast relaxation processes (the lifetime of an excited state is much shorter than the modulation period), the optical to thermal energy conversion efficiency is given in the modified form

$$\eta_{\text{NR}}^{(e)}(\hbar\Omega, T) = 1 - \eta_R(\hbar\Omega, T) \frac{\hbar\Omega_{\text{em}}}{\hbar\Omega} \quad (5)$$

where $\hbar\Omega_{\text{em}}$ is the emission photon energy and $\eta_R(\hbar\Omega, T)$ is the quantum efficiency of the system. The nonradiative energy conversion quantum efficiency [$\eta_{\text{NR}}^{(e)}(\hbar\Omega, T)$] is given by

$$\eta_{\text{NR}}(\hbar\Omega, T) = 1 - \eta_R(\hbar\Omega, T). \quad (6)$$

In a weak absorption limit ($\beta\mu_s \ll 1$) and under assumption that the thermal expansion coefficient and the sample thickness are small enough, the second term in Eq. (1) can be neglected and Eq. (1) is now simplified to

$$P(\hbar\Omega) = AI_0(\hbar\Omega) \eta_{\text{NR}}^{(e)}(\hbar\Omega, T) \beta(\hbar\Omega), \quad (7)$$

where A is the apparatus correction factor independent of the excitation energy.

After taking into account the spectral intensity distribution of the used light source and calibrating the photoacoustic spectrum of the sample with a reference of the PAS signal from glassy carbon the measured PAS signal amplitude [$Q_{\text{PAS}}(\hbar\Omega)$] is described by

$$Q_{\text{PAS}}(\hbar\Omega) = A \eta_{\text{NR}}^{(e)}(\hbar\Omega, T) \beta(\hbar\Omega). \quad (8)$$

Thus, $\eta_{\text{NR}}^{(e)}(\hbar\Omega, T)$ can be obtained from Eq. (8) if $\beta(\hbar\Omega)$ is determined from another independent experiment. $\eta_{\text{NR}}(\hbar\Omega, T)$ and $\eta_R(\hbar\Omega, T)$ can be determined subsequently by the use of Eqs. (5) and (6).

IV. SAMPLE PREPARATION AND ANNEALING TREATMENTS

YAG:Cr,Mg single crystals with a diameter of ~ 10 mm were grown by a Czochralski method and grown in a mixed atmosphere of 97% N_2 and 3% O_2 along the [111] direction with a growing rate of 2 mm/h. A magnesium metal ion was used as a compensating ion to form tetravalent chromium ions in the host lattice. Calcium metal ion is sometime also used for this purpose. Since Mg^{2+} ion has a much smaller ionic radius than Ca^{2+} ion, it preferentially substitutes octahedral Al^{3+} sites to promote forming Cr^{4+} ion at tetrahedral Al^{3+} sites.

The single crystal samples used for PAS and optical absorption measurements were cut in a direction perpendicular to the growing axis and with a thickness of ~ 1 mm. Their crystal surfaces were gradually polished up to the optical quality.

In addition to as-grown crystal samples, we used high-temperature annealing treatments to modify relative concentrations of Cr^{3+} and Cr^{4+} ions in YAG crystals. A H_2 -annealed sample was obtained at 1200 °C for 10 h and a air-annealed sample at 1400 °C for 2 h. Previous experiments performed by Ubizskii *et al.*²¹ showed that these annealing treatment conditions sufficiently provide a complete saturation in chromium recharging processes.

The total chromium content of YAG:Cr,Mg samples used for this work was determined by the absorption band intensity of Cr^{3+} in the H_2 -annealed sample. First, the Cr^{3+} con-

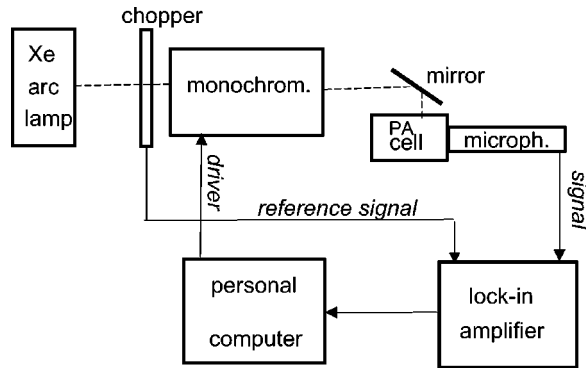


FIG. 2. Schematic PAS setup.

centration of a YAG:Cr³⁺ sample used as a reference was determined by a chemical analysis and we then compared the absorption band intensities of the referenced YAG:Cr³⁺ sample and the H₂-annealed YAG:Cr,Mg sample to obtain the total Cr content of $\sim 2 \times 10^{20} \text{ cm}^{-3}$ in YAG:Cr,Mg.²¹ The Cr⁴⁺ concentration in our present YAG:Cr,Mg samples was estimated to be $\sim 4 \times 10^{17} \text{ cm}^{-3}$ by comparing the intensity of a characteristic absorption band near 1 μm with the absorption data reported in the literature.²²

V. EXPERIMENTS AND RESULTS

Optical absorption spectra were measured with a Carl Zeiss Jena spectrometer. Visible and near-infrared luminescence measurements were performed with two separate setups. For the visible measurements, luminescence was dispersed by a 2 m monochromator adapted by a spectrograph (Carl Zeiss Jena PGS2 with a 651 grooves/mm grating) and detected by a photon counting technique (a Hamamatsu R943-02 photomultiplier tube). For the near-infrared measurements, luminescence was dispersed by a 1 m spectrometer (SPEX 1704) and detected by a standard lock-in technique (a liquid nitrogen cooled germanium detector). An argon laser working in a single line mode was used as an excitation source. Low-temperature experiments at 20 K were performed using a closed cycle helium refrigerator (APD Cryogenic INC HC4).

Photoacoustic spectroscopy measurements were carried out using a single beam spectrometer presented in Fig. 2. A xenon arc lamp (XBO 900) was used as a light source. A frequency-variable chopper was used to generate periodic light amplitudes. A computer-controlled monochromator (SPM2 with a grating 600 grooves/mm) equipped with a non-resonant photoacoustic detector (PAC 300, MTEC, USA). A sample compartment made of brass and with entrance and exit quartz windows is referred to a photoacoustic cell (PAC). A dual phase lock-in amplifier (SR850) driven by a computer was employed to complete PAS registration and data acquisition and to measure in-phase and out-of phase components of PAS signals simultaneously.

Figures 3(a) and 3(b) show luminescence and absorption spectra of as-grown, air-annealed, and H₂-annealed YAG:Cr,Mg. Red luminescence (13 200–15 400 cm^{-1}) occurred in all the samples and is attributed to the ${}^2E \rightarrow {}^4A_2$

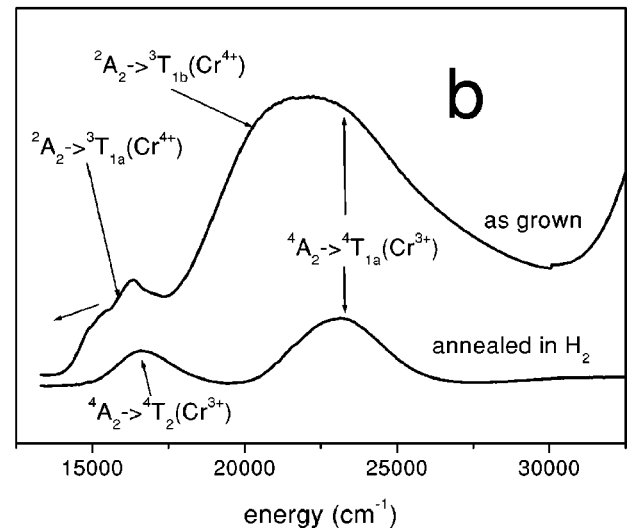
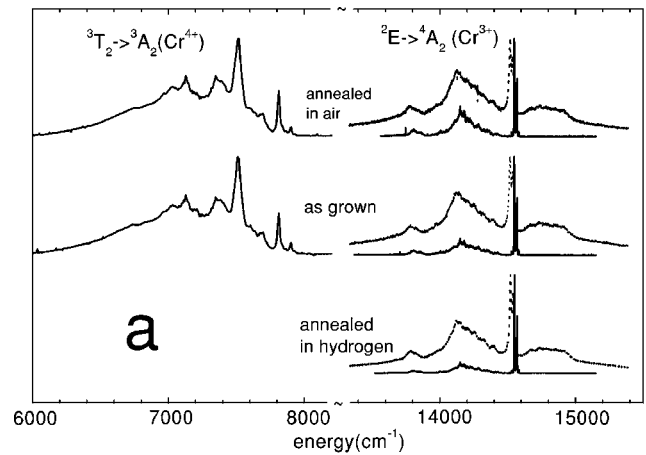


FIG. 3. (a) Room temperature (dotted curves) and 20 K (solid curves) luminescence spectra and (b) room temperature absorption spectra of as-grown and H₂-annealed YAG:Cr,Mg crystal samples.

transition of Cr³⁺ accompanying Stokes and anti-Stokes phonon sidebands. NIR luminescence (6000–8000 cm^{-1}) occurred only in as-grown and air-annealed YAG:Cr,Mg and is attributed to the ${}^3T_2 \rightarrow {}^3A_2$ transition of Cr⁴⁺. H₂-annealed YAG:Cr,Mg exhibited only two ${}^4A_2 \rightarrow {}^4T_2$ and ${}^4T_{1a}$ absorption bands of Cr³⁺ [Fig. 3(b)] and as-grown YAG:Cr,Mg exhibited a superposition of Cr³⁺ absorption bands (${}^4A_2 \rightarrow {}^4T_2$ and ${}^4T_{1a}$) and Cr⁴⁺ absorption bands (${}^3A_2 \rightarrow {}^3T_{1a}$ and ${}^3T_{1b}$).

For our PAS experiments, we carefully considered the following factors that significantly influence the accuracy and analysis of PAS data. First, we discuss the validity of a weak absorption limit ($\beta\mu_s \ll 1$). The thermal diffusivity of YAG single crystals experimentally reported for $3.66 \times 10^{-2} \text{ cm}^2/\text{s}$.²³ When a modulation frequency of 60 Hz is used for PAS experiments, the thermal diffusion length of YAG is obtained for $\mu_s \approx 10^{-2} \text{ cm}$ using Eq. (3). Since the optical absorption coefficients (β) of both Cr³⁺ and Cr⁴⁺ ions in the YAG:Cr,Mg samples used for this study do not exceed 15 cm^{-1} , the weak absorption limit of $\beta\mu_s \ll 1$ is fulfilled and Eq. (8) is reasonably applicable to our sample systems.

Second, existing theories describe photoacoustic effects within a one-dimension approximation. However, the effects of heat flowing in three dimensions (3D) become important in some material systems.²⁴ Due to this effect critical frequency dependent on a cell diameter and thermal diffusivity of a filling gas emerges. Below this frequency one-dimensional theories are not valid. Recently, Jones and McClelland²⁵ have examined 3D effects for different materials and for different distances from entrance window with photoacoustic cell (PAC300, MTEC USA) filled with helium gas. They have shown that even the PAS signal has been disturbed by 3D effects the correct quantitative results can be obtained based on a one-dimensional model provided that all measurements are related to a proper reference sample. To minimize the 3D effects in our PAS experiments, we filled a PAC with air because air has a lower thermal diffusivity than He gas. To check the influence of the 3D effect we have measured the dependence of the PAS amplitude on modulation frequency for the glassy carbon sample of the same shape as sample under investigation. Since dependence we have obtained was in full accordance with one dimensional model²⁶ we have assumed that the 3D effects are negligible in our PAS experiments.

Last, we considered the absorption from PAC windows and walls. For each of our PAS experiments, we first measured a blank PAS spectrum of the used PAC. The blank PAS spectrum as the background was subtracted from the measured PAS spectrum of the sample (X 's and Y 's represent in-phase and out-of-phase components of the sample, respectively). Blank in-phase components (X_b) and out-of-phase components (Y_b) of the PAC were first measured with a polished quartz disc placed in the PAC (the quartz disc thickness was 1.5 mm similar to the thickness of our YAG:Cr,Mg samples). A PAS signal vector magnitude (Q_{PAS}) can be defined by the in-phase and out-of-phase components of PAS signals as follows:

$$Q_{PAS} = \sqrt{(X_s - X_b)^2 + (Y_s - Y_b)^2} = \sqrt{X_{cor}^2 + Y_{cor}^2} \quad (9)$$

Corrected PAS spectra of as-grown, air-annealed, and H₂-annealed YAG:Cr,Mg samples are presented in Figs. 4(a)–4(c), respectively. Absorption spectra of these samples are also given in the right axis of Figs. 4(a)–4(c). For the H₂-annealed sample, an excitation spectrum of the ²E → ⁴A₂ luminescence is also presented in Fig. 4(c).

VI. DISCUSSION

A. Cr⁴⁺ case

From Figs. 4(a) and 4(b), we see that both as-grown and air-annealed YAG:Cr,Mg samples exhibit a constant ratio of the PAS signal amplitude to the absorption coefficient over a spectral range of 400–800 nm. This indicates, using Eq. (8), that the optical to thermal energy conversion efficiency [$\eta_{NR}^{(e)}(\hbar\Omega)$] is independent of the excitation energy ($E_{ex} = \hbar\Omega$) in both samples that contained Cr⁴⁺ ions and exhibited strong Cr⁴⁺ absorption bands [~ 620 nm for ³A₂ → ³T_{1a} and ~ 480 nm for ³T_{1b} in Figs. 3(b), 4(a), and 4(b)].

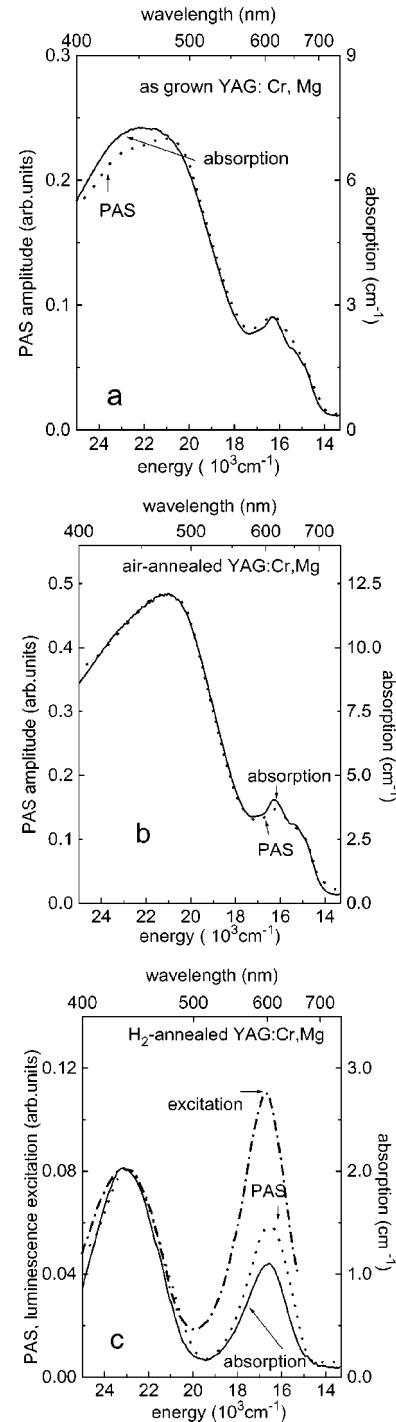


FIG. 4. PAS and absorption spectra of (a) as-grown, (b) air-annealed, (c) H₂-annealed YAG:Cr,Mg samples at room temperature. A room temperature excitation spectrum of ²E → ⁴A₂ luminescence of Cr³⁺ for the H₂-annealed sample is also included in (c).

From the configurational coordinate diagram of Cr⁴⁺ in Fig. 1(a), one can clearly see that the thermal barrier (E_{nr}) of the ³T₂ first excited state of Cr⁴⁺ is much lower relative to the Cr³⁺ case in Fig. 1(b). At room temperature, both the thermal energy conversion efficiency ($\eta_{NR}^{(e)}$) and the nonradiative energy conversion quantum efficiency (η_{NR}) are close to 1 in our two Cr⁴⁺ contained systems.

B. Cr³⁺ case

When looking at the pure Cr³⁺ case in Fig. 4(c) (YAG:Cr,Mg annealed in H₂), we found that the optical to thermal energy conversion efficiency ($\eta_{NR}^{(e)}$) is excitation-energy dependent between 400–800 nm. For the sake of intuition, we rewrite Eq. (8) in the form

$$\eta_{NR}^{(e)}(\hbar\Omega) \propto \frac{Q_{PAS}(\hbar\Omega)}{\beta(\hbar\Omega)}. \quad (10)$$

Using Eq. (10) and the PAS and absorption data presented in Fig. 4(c), we obtained $\eta_{NR}^{(e)}(438 \text{ nm}) \approx 0.7 \eta_{NR}^{(e)}(600 \text{ nm})$. We therefore expect from Eqs. (5) and (6) that the quantum efficiency (η_R) of Cr³⁺ increases with decreasing excitation wavelength (increasing excitation energy E_{ex}).

Since high-field Cr³⁺ ion has a long-lived emitting state (²E), both fast and slow relaxation processes occur simultaneously. In this case, Eq. (5) cannot be reasonably applied to the prediction of the PAS effects in our H₂-annealed YAG:Cr,Mg sample and a new model should generally consider nonradiative relaxation processes with fast heat components (Q_e) and slow heat components (Q_m). The fast heat components are produced by excited ions relaxing from their short-lived states (⁴T_{1a} and/or ⁴T₂) via the fast interconfigurational relaxation to their long-lived ²E state [Fig. 1(b)]. The slow heat components are released via the slow intracoufigurational relaxation starting with the long-lived ²E state. Ouzafe *et al.*²⁷ have studied photoacoustic effects in a molecular system that contains two heat sources corresponding to nonradiative relaxation processes of two different excited states with significantly different lifetimes and obtained PAS signals in the following complex form:

$$P = Q_{PAS} \exp i(2\pi ft + \phi), \quad (11)$$

where the amplitude of PAS signals (Q_{PAS}) is

$$Q_{PAS} = A \frac{I_0 \beta \mu_s Q_e}{4\pi f E_{ex} \alpha_s \sqrt{(\beta \mu_s + 1)^2 + 1}} \times \left\{ 1 + \frac{2 \left(\frac{Q_e}{Q_m \eta_{NR}} \right) + 1}{\left(\frac{Q_e}{Q_m \eta_{NR}} \right)^2 [1 + (2\pi f \tau_m)^2]} \right\}^{1/2} \quad (12)$$

and the phase of PAS signals (ϕ) is

$$\phi = -\pi + \arctan(\beta \mu_s + 1) - \arctan \left\{ \frac{2\pi f \tau_m}{1 + \left(\frac{Q_e}{Q_m \eta_{NR}} \right) [1 + (2\pi f \tau_m)^2]} \right\}. \quad (13)$$

Here τ_m is the lifetime of the long-lived excited state. We have considered that for the Cr³⁺ system we have two step relaxation, the first, fast nonradiative relaxation from E_e state to the E_m state (²E), and then the second, slow radiative or nonradiative process that ends in the ground state, thus $E_{ex} = Q_e + Q_m$. Upon application of Eqs. (11)–(13), we have

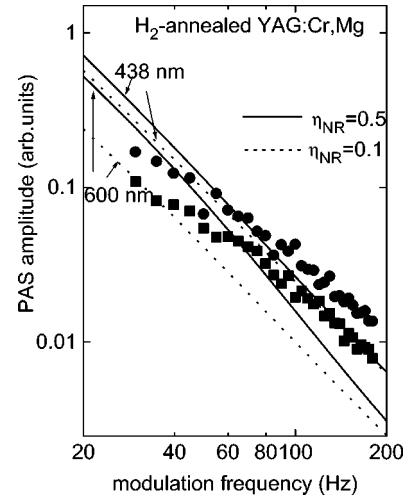


FIG. 5. Calculated and experimental PAS amplitudes as a function of modulation frequency (f) for 438 and 600 nm absorption bands of Cr³⁺ in the H₂-annealed YAG:Cr,Mg sample.

calculated the PAS amplitude as a function of the modulation frequency (f) for two absorption bands of Cr³⁺ [peaked at ~ 438 and ~ 600 nm in Fig. 4(c)]. Calculations have been performed for two cases, assuming $\eta_{NR} = 0.5$ and $\eta_{NR} = 0.1$. In both cases we used the quantity of the lifetime of the ²E excited state of Cr³⁺, $\tau_m = 3$ ms. Our results are illustrated in Fig. 5 (solid lines for $\eta_{NR} = 0.5$ and dotted lines for $\eta_{NR} = 0.1$). One can clearly see that the PAS amplitudes for both bands vary with the modulation frequency in the same way. The PAS amplitudes of the H₂-annealed YAG:Cr,Mg sample at ~ 438 nm ($E_{ex} = 22830 \text{ cm}^{-1}$) and ~ 600 nm ($E_{ex} = 16670 \text{ cm}^{-1}$) as a function of the modulation frequency (f) were experimentally determined (solid circles and squares in Fig. 5). It can be seen that although calculated slopes and intensities differ from measured characteristics, qualitative agreement between theory and experiments exists.

Using Eq. (12), one obtains the optical to thermal energy conversion efficiency ($\eta_{NR}^{(e)}$) for the system with a long-lived excited state such as the ²E excited state of Cr³⁺ given by

$$\eta_{NR}^{(e)} \propto \left\{ \left(\frac{E_{ex} - Q_m}{E_{ex}} \right)^2 + \frac{2 \left(\frac{E_{ex} - Q_m}{E_{ex}} \right) \left(\frac{Q_m \eta_{NR}}{E_{ex}} \right) + \left(\frac{Q_m \eta_{NR}}{E_{ex}} \right)^2}{1 + (2\pi f \tau_m)^2} \right\}^{1/2}. \quad (14)$$

Figure 6 presents calculated results for the optical to thermal energy conversion efficiency ($\eta_{NR}^{(e)}$) as a function of the excitation energy (E_{ex}) using Eq. (14) and $f = 60$ Hz as well as with a constant optical to thermal energy conversion quantum efficiency for a set of $\eta_{NR} = 0.0, 0.2, 0.4, 0.6, 0.8, 1.0$. From Fig. 6, we notice that $\eta_{NR}^{(e)}$ for all cases increases with increasing excitation energy (E_{ex}). One possibility to have a

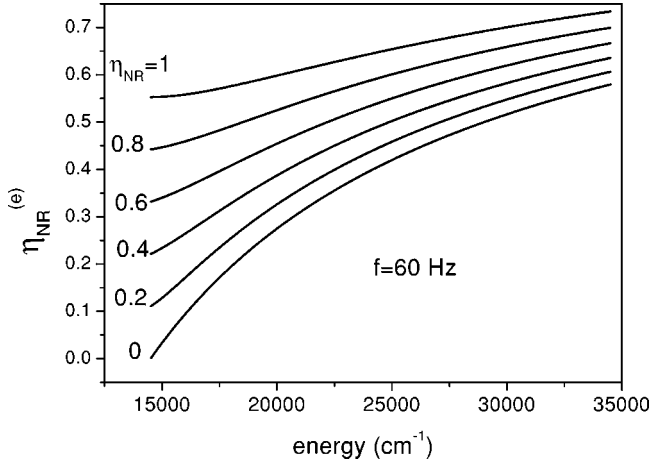


FIG. 6. Calculated nonradiative energy conversion efficiency as a function of excitation energy ($E_{\text{ex}} = \hbar\Omega$) based on Eq. (14).

decrease in $\eta_{NR}^{(e)}$ with E_{ex} is to assume that the energy conversion efficiency (η_{NR}) decreases with increasing excitation energy (E_{ex}). This is a reason why we will discuss the details of nonradiative internal conversion processes in luminescent centers below.

C. Modeling of nonradiative relaxation processes

The quantum efficiency of an optically activated material system can be described in the context of the configurational coordinate model (Fig. 7). When the system is excited from its ground state (g) to a vibronic state ($|e, n\rangle$, E_e^n) of its excited electronic manifold (e) with a photon of $\hbar\Omega$, two nonradiative relaxation processes occur. One is an intraconfigurational relaxation process from $|e, n\rangle$ down to $|e, n-1\rangle$ that emits a phonon with a probability of $p_{\text{intra}}^n(e)$ and

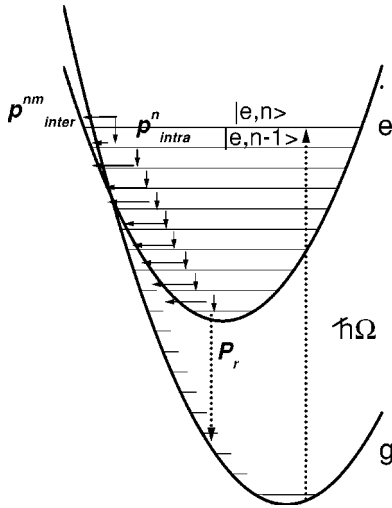


FIG. 7. Configurational coordinate diagram. Solid and dashed arrows represent nonradiative and radiative processes, respectively. p_{intra}^n , p_{inter}^{nm} , and p_r represent the probability of the intraconfigurational and interconfigurational nonradiative relaxation processes, and the radiative process, respectively. $\hbar\Omega$ denotes the excitation energy.

another is an interconfigurational nonradiative internal relaxation process that transforms the system without losing the energy ($E_e^n = E_g^m$) from $|e, n\rangle$ to $|g, m\rangle$ with a probability of $p_{\text{inter}}^{nm}(e \rightarrow g)$. Upon a steady-state excitation of $I_0(\hbar\Omega)$ with an absorbed power of $\beta(\hbar\Omega)I_0(\hbar\Omega)$, we can obtain a set of rate equations describing the kinetics of deexcitation processes and calculate the quantum efficiency (η_R) of the system in Fig. 7 by¹²

$$\eta_R(\hbar\Omega, T) = \left[\prod_{k=1}^{n(\hbar\Omega)} \frac{p_{\text{intra}}^k(e)}{p_{\text{intra}}^k(e) + p_{\text{inter}}^{kl}(e \rightarrow g)} \right] \left[\frac{p_R^i}{p_R^i + p_{NR}^i(T)} \right], \quad (15)$$

where p_R^i and p_{NR}^i are the probability of radiative and non-radiative processes, respectively, in a thermalized system. In Eq. (15), the term in the first brackets describes fast processes before thermalization and the term in the second bracket describes slow processes after thermalization. The slow processes are temperature-dependent because the probability of nonradiative processes in the thermalized system is a function of temperature in the following form:

$$p_{NR}^i(T) = \frac{\sum_n p_{\text{inter}}^{nm}(e \rightarrow g) \exp(-E_e^n/kT)}{\sum_n \exp(-E_e^n/kT)}. \quad (16)$$

It is straightforward to see that the total probability of all the fast processes decreases with increasing excitation energy ($\hbar\Omega$). If $\hbar\Omega_2 > \hbar\Omega_1$,

$$\begin{aligned} & \prod_{k=1}^{n_2(\hbar\Omega_2)} \frac{p_{\text{intra}}^k(e)}{p_{\text{intra}}^k(e) + p_{\text{inter}}^{kl}(e \rightarrow g)} \\ &= \left[\prod_{k=1}^{n_1(\hbar\Omega_1)} \frac{p_{\text{intra}}^k(e)}{p_{\text{intra}}^k(e) + p_{\text{inter}}^{kl}(e \rightarrow g)} \right] \\ & \times \prod_{i>n_1}^{n_2(\hbar\Omega_2)} \frac{p_{\text{intra}}^i(e)}{p_{\text{intra}}^i(e) + p_{\text{inter}}^{il}(e \rightarrow g)} \\ & < \prod_{k=1}^{n_1(\hbar\Omega_1)} \frac{p_{\text{intra}}^k(e)}{p_{\text{intra}}^k(e) + p_{\text{inter}}^{kl}(e \rightarrow g)}. \end{aligned} \quad (17)$$

As extrapolated directly from this inequality, the quantum efficiency of the system described by Eq. (15) decreases with increasing excitation energy. As a consequence, the nonradiative energy conversion efficiency ($\eta_{NR}^{(e)}$) is expected from Eq. (5) to have $\eta_{NR}^{(e)}(\hbar\Omega_2) > \eta_{NR}^{(e)}(\hbar\Omega_1)$ for $\hbar\Omega_2 > \hbar\Omega_1$. In the special case when a system has 0% quantum efficiency, its optical to thermal energy conversion efficiency is $\hbar\Omega$ independent. This is our Cr^{4+} case [Figs. 4(a) and 4(b)].

Our Cr^{3+} case in Fig. 4(c) showed that the ~ 600 nm absorption (${}^4A_2 \rightarrow {}^4T_2$) is weaker than the ~ 438 nm absorption band (${}^4A_2 \rightarrow {}^4T_{1a}$) whereas the ~ 600 nm excitation band (${}^4A_2 \rightarrow {}^4T_2$) is stronger than the ~ 438 nm excitation band (${}^4A_2 \rightarrow {}^4T_{1a}$). From the excitation spectrum, the quantum efficiency of our Cr^{3+} system is expected to be greater

upon excitation into the lower energy 4T_2 quartet state than into the higher energy ${}^4T_{1a}$ quartet state of Cr^{3+} . The ratio of the excitation spectrum to the absorption coefficient of Cr^{3+} [Fig. 4(c)] yields the direct information about the non-radiative internal conversion processes in the excited states of the Cr^{3+} system. Actually, this ratio for the ${}^4A_2 \rightarrow {}^4T_{1a}$ band is smaller by a factor of 0.37 than that for the ${}^4A_2 \rightarrow {}^4T_2$ band. Such a fact indicates that the nonradiative energy conversion efficiency ($\eta_{\text{NR}}^{(e)}$) increases with increasing excitation energy, even faster than the result predicted by Eq. (14) (Fig. 6). As far as we have considered the above-formulated theory that describes the relaxation processes in a system such as our present Cr^{3+} system, it cannot predict a decrease in the optical to thermal energy conversion efficiency ($\eta_{\text{NR}}^{(e)}$) with excitation energy ($\hbar\Omega$). We will develop and discuss a generalized theory that concerns the presence of spatial energy migration processes in our forthcoming paper.

VII. CONCLUSIONS

We have analyzed the nonradiative processes in the Cr^{4+} and Cr^{3+} systems in different YAG:Cr,Mg crystals. The analysis of the PAS and optical absorption spectra yielded the conclusion that the quantum efficiency of Cr^{4+} in as-grown and air-annealed YAG:Cr,Mg samples is very weak (at room temperature, almost all energy is transformed into heat). It is much less than that obtained by Kück *et al.*¹⁹ where the quantum efficiency of YAG:Cr⁴⁺ has been estimated as 0.5 for helium temperature and 0.2 for room temperature. We have found that PAS spectra of the YAG:Cr⁴⁺ system can be analyzed using the standard Rosencwaig-Gersho theory that relates PAS to absorption coefficient by relation (7).

A very interesting result has been obtained in the case of the sample annealed in hydrogen [Fig. 4(c)]. Actually, this sample contains only Cr^{3+} centers. We see that the ratio of PAS amplitude to the absorption coefficient decreases with increasing of excitation energy. One can also see that this effect is directly related to Cr^{3+} from analysis of the as-grown sample. Here we deal with Cr^{3+} and Cr^{4+} and what is seen from the double absorption bands in the higher energy region. One can see that for the energy $22\,830\text{ cm}^{-1}$, where we expect the absorption band related to the ${}^4A_2 \rightarrow {}^4T_{1a}$ tran-

sition in the Cr^{3+} system the PAS signal is smaller than the absorption.

Considering the ratio of photoacoustic amplitude signal to the absorption coefficient in the case of the Cr^{3+} system in the framework of the standard approach one obtains decreasing of optical to thermal energy conversion efficiency with increasing of excitation energy. On the other hand, our analysis of nonradiative processes in the luminescence center has shown that such an effect is impossible. The increasing of the probability of the nonradiative internal conversion process with increasing excitation energy is also obtained from comparison of the absorption and excitation spectra.

Thus, the specific ratio of the PAS to absorption in the case of the Cr^{3+} system has to be related to more complicated phenomena. In all samples we have approximately the same quantity of chromium. In the as-grown sample and in the sample annealing in air the dominant dopant was Cr^{4+} . In the sample annealed in hydrogen atmosphere all chromium ions were reduced to Cr^{3+} (no Cr^{4+} was detected). Only Cr^{3+} has a metastable 2E state that is characterized by a lifetime of 3 ms. Since the 2E state is characterized by very weak electron-lattice coupling no the Stokes shift between absorption and emission is noticed. Thus although the absorption ${}^4A_2 \rightarrow {}^2E$ is weak the resonance excitation energy transfer between isolated chromium is possible. One should notice that in the case of the Cr^{4+} ion the first excited state is 3T_2 , which is rather strongly coupled to the lattice. In addition this is not the metastable state due to the quite high probability of radiative and nonradiative processes. The 3T_2 lifetime is of the range of μs .¹⁹ As a result the spatial excitation energy migration between Cr^{4+} is much less effective than between the Cr^{3+} ions of the same concentration. In the next paper we provide the model of the energy migration to the surface that explains our experimental results.²⁸

ACKNOWLEDGMENTS

The Authors express their great gratitude to Dr. Z. Frukacz (Institute for Electronic Materials Technology, Warsaw, Poland) and Dr. I. Solskii (R&D Institute for Materials, SRC "Carat," Lviv, Ukraine) for growing single crystals of YAG:Cr,Mg, and also to Dr. B. Kuklinski for measuring the excitation spectra. This study has been supported by the Polish Committee for Scientific Research (Grant No. 7T07B04918).

¹A. P. Shkadarevich, in *Tuneable Solid State Lasers*, OSA Proceedings Series Vol. 5, edited by M. L. Shand and H. P. Jensen (OSA, Washington, DC, 1989), p. 60; G. M. Zverev and A. V. Shestakov, *ibid.*, p. 66.

²A. G. Okhrimchuk and A. V. Shestakov, *Opt. Mater.* **3**, 1 (1994).

³S. Kück, K. Petermann, U. Pohlmann, and G. Huber, *J. Lumin.* **68**, 1 (1996).

⁴M. Grinberg, A. Sikorska, and S. Kaczmarek, *J. Alloys Compd.* **300-301**, 158 (2000).

⁵A. Sliwinski, M. Grinberg, and A. Sikorska, *Mol. Quantum Acoustics* **22**, 261 (2001).

⁶M. Grinberg, A. Sikorska, B. Kuklinski, and S. Zachara, in *Xth International Conference on Photoacoustic and Photothermal Phenomena, 27–29 August 1998, Rome*, edited by F. Suderi and M. Bertolotti [AIP Conf. Proc. **463**, 241 (1998)].

⁷A. Sliwinski, M. Grinberg, and A. Sikorska, *Proc. SPIE* **4514**, 166 (2001).

⁸A. Sikorska, *Proc. SPIE* **4514**, 179 (2001).

⁹A. Sliwinski, M. Grinberg, and A. Sikorska, in *2001 IEEE Ultrasonics Symposium, October 7–10, 2001, Atlanta, Georgia*, edited by D. E. Yuhas and S. C. Scheider [Proc.-IEEE Ultrason. Symp. **CH7263**, 419 (2002)].

- ¹⁰M. Grinberg, A. Mandelis, K. Fjeldsted, and A. Othonos, *Phys. Rev. B* **48**, 5922 (1993).
- ¹¹M. Grinberg, A. Mandelis, and K. Fjeldsted, *Phys. Rev. B* **48**, 5935 (1993).
- ¹²M. Grinberg and A. Mandelis, *Phys. Rev. B* **49**, 12 496 (1994).
- ¹³A. Rosencwaig and A. Gresho, *J. Appl. Phys.* **47**, 64 (1976).
- ¹⁴B. Henderson and G. F. Imbusch, *Optical Spectroscopy of Inorganic Solids* (Clarendon, Oxford, 1989).
- ¹⁵B. Struve and G. Huber, *Appl. Phys. B: Photophys. Laser Chem.* **36**, 195 (1985).
- ¹⁶S. Kück, *Appl. Phys. B: Lasers Opt.* **72**, 515 (2001).
- ¹⁷Y. R. Shen and K. L. Bray, *Phys. Rev. B* **56**, 10 882 (1997).
- ¹⁸M. Grinberg, *J. Lumin.* **54**, 369 (1993).
- ¹⁹S. Kück, K. Petermann, U. Pohlmann, and G. Huber, *Phys. Rev. B* **51**, 17 323 (1995).
- ²⁰F. McDonald and G. Wetsel, *J. Appl. Phys.* **49**, 2313 (1978).
- ²¹S. B. Ubizskii, S. S. Melnyk, B. V. Padlyak, A. O. Matkowskii, A. Jankowska-Frydel, and Z. Frukacz, *Proc. SPIE* **4412**, 63 (2001).
- ²²V. M. Garmash, V. A. Zhitnyuk, A. G. Okhrimchuk, and A. V. Shestakov, *Izv. Akad. Nauk SSSR, Neorg. Mater.* **26**, 1700 (1990).
- ²³W. F. Krupke, M. D. Shinn, J. E. Marion, J. A. Caird, and S. E. Stokowski, *J. Opt. Soc. Am. B* **3**, 102 (1986).
- ²⁴R. S. Quimby and W. M. Yen, *Appl. Phys. Lett.* **35**, 43 (1979).
- ²⁵R. W. Jones and J. F. McClelland, *Appl. Spectrosc.* **55**, 1360 (2001).
- ²⁶L. C. Aamondt, J. M. Murphy, and J. G. Parker, *J. Appl. Phys.* **48**, 927 (1977).
- ²⁷M. Ouzafe, P. Poulet, and J. Chambron, *Photochem. Photobiol.* **55**, 491 (1992).
- ²⁸M. Grinberg, A. Sikorska, and A. Sliwinski, *Phys. Rev. B* **67**, 045114 (2003).